Biochimica et Biophysica Acta 1818 (2012) 194–204

Contents lists available at SciVerse ScienceDirect

Biochimica et Biophysica Acta

journal homepage: www.elsevier.com/locate/bbamem

Mechanism of structural transformations induced by antimicrobial peptides in lipid membranes ☆

Kin Lok H. Lam [a,b,1], Hao Wang [c,1], Ting Ann Siaw [b,d], Matthew R. Chapman [b,d], Alan J. Waring [e,f], James T. Kindt [c], Ka Yee C. Lee [b,d,*]

[a] Department of Physics, The University of Chicago, Chicago, IL, USA
[b] Institute for Biophysical Dynamics & James Franck Institute, The University of Chicago, Chicago, IL, USA
[c] Department of Chemistry, Emory University, Atlanta, GA, USA
[d] Department of Chemistry, The University of Chicago, Chicago, IL, USA
[e] Los Angeles Biomedical Research Institute at Harbor-UCLA Medical Center, Torrance, CA, USA
[f] Department of Physiology and Biophysics, School of Medicine, University of California at Irvine, Irvine, CA, USA

ARTICLE INFO

Article history:
Received 2 August 2011
Received in revised form 1 November 2011
Accepted 2 November 2011
Available online 9 November 2011

Keywords:
Membrane disruption mechanism
Phospholipid
Protegrin-1
Atomic force microscopy
Molecular dynamics
Pore formation

ABSTRACT

It has long been suggested that pore formation is responsible for the increase in membrane permeability by antimicrobial peptides (AMPs). To better understand the mechanism of AMP activity, the disruption of model membrane by protegrin-1 (PG-1), a cationic antimicrobial peptide, was studied using atomic force microscopy. We present here the direct visualization of the full range of structural transformations in supported lipid bilayer patches induced by PG-1 on zwitterionic 1,2-dimyristoyl-snglycero-phospho-choline (DMPC) membranes. When PG-1 is added to DMPC, the peptide first induces edge instability at low concentrations, then pore-like surface defects at intermediate concentrations, and finally wormlike structures with a specific length scale at high concentrations. The formation of these structures can be understood using a mesophase framework of a binary mixture of lipids and peptides, where PG-1 acts as a line-active agent. Atomistic molecular dynamics simulations on lipid bilayer ribbons with PG-1 molecules placed at the edge or interior positions are carried out to calculate the effect of PG-1 in reducing line tension. Further investigation of the placement of PG-1 and its association with defects in the bilayer is carried out using unbiased assembly of a PG-1 containing bilayer from a random mixture of PG-1, DMPC, and water. A generalized model of AMP induced structural transformations is also presented in this work. This article is part of a Special Issue entitled: Membrane protein structure and function.

1. Introduction

A central paradigm of modern molecular biology is the mutual dependence of structure and function. Thus, discovering the structure of a biological system often leads to the understanding of its function. For example, membrane fusion protein has a strongly curved intrinsic shape, and, when coated on a membrane, can distort the initial shape of the membrane surface, driving its fusion with an opposing membrane [1]. In an opposite manner, the formation of vesicles out of plasma membranes and trans-Golgi membranes is attributed to the adsorption of proteins with an intrinsic shape opposite to that of the membrane fusion protein [2–5]. Consequently, the shape of the membrane is controlled not only by the mechanical properties of the lipid bilayer itself [6], but also to a large extent by proteins that are embedded or associated with the lipid membrane [7]. The inclusion of proteins in a membrane can cause a lipid bilayer to undergo structural transformations, turning the original planar geometry into a variety of mesophases [8]. The equilibrium configuration of a membrane is determined by minimizing its free energy, which in turn is subject to perturbations dictated by the molecular details of the inclusion [9].

A special class of membrane inclusion proteins is that of the antimicrobial peptide (AMP). These peptides have been shown to kill bacteria by increasing the membrane's permeability to ions or larger molecules [10–16]. It has long been proposed that the lytic effect of AMPs stems from their ability to induce structural changes in the membrane, resulting in pore formation [10–16]. Therefore, one can

Abbreviations: AMP, AntiMicrobial Peptide; PG-1, Protegrin-1; AFM, Atomic Force Microscopy; DHPC, 1,2-dihexanoyl-*sn*-glycero-3-phospho-choline; DMPC, 1,2-dimyristoyl-*sn*-glycero-3-phospho-choline; SDS, sodium-dodecyl-sulfate; DPC, dodecyl-phospho-choline; POPC, palmitoyl-oleoylphosphatidyl-choline; POPG, palmitoyl-oleoylphosphatidyl-glycerol; NMR, Nuclear Magnetic Resonance; C_b, bulk peptide concentration; C_b^*, critical bulk peptide concentration; GROMACS, Groningen Machine for Chemical Simulations; MD, Molecular Dynamics

☆ This article is part of a Special Issue entitled: Membrane protein structure and function.

* Corresponding author at: Department of Chemistry, The University of Chicago, 929 E. 57th Street, Chicago, IL 60637, USA. Tel.: +1 773 702 7068; fax: +1 773 702 0805.
E-mail address: kayeelee@uchicago.edu (K.Y.C. Lee).

[1] Equally contributed to this work.

0005-2736/$ – see front matter © 2011 Elsevier B.V. All rights reserved.
doi:10.1016/j.bbamem.2011.11.002

gain insight into the breakdown of the membrane as a permeability barrier if one can better understand what dictates the mixed assembled structure resulting from such lipid–peptide interactions. For instance, it has been suggested that the resulting pore structure can be barrel-stave-like [10–12,14] or toroidal-like [13,15,16], depending on the specific peptide, though direct observation of such pores on membranes has been difficult. Protegrin-1 (PG-1) is an AMP from porcine leukocytes that has only 18 amino acids (NH_2-RGGRLCYCRRRFCVCVGR-$CONH_2$), and a net charge of +6 due to the six arginine residues in the sequence. It exhibits antimicrobial activity over a wide range of bacteria including *Escherichia coli*, *Listeria monocytogenes*, and *Neisseria gonorrheae*. In recent years, pore formation induced by PG-1 on supported lipid bilayer patches has been directly visualized using atomic force microscopy (AFM) [17]. In addition to pores, increasing PG-1 concentration has led to other unique types of lipid–peptide assembled structures. The spectrum of structural transformations observed with increasing PG-1 concentration progresses from bilayer edge instability, to pore formation at the center of the bilayer patch, and finally to a network of wormlike structures [17]. These higher degrees of structural transformations also agree with a number of observations whereby wormlike protrusions from the cell membrane have been observed when the cells are incubated with AMPs [18–20].

The rich mesophase behavior in membranes containing PG-1 is reminiscent of a classic amphiphilic system involving a binary mixture of short- and long-chain lipids such as 1,2-dihexanoyl-*sn*-glycero-3-phospho-choline (DHPC) and 1,2-dimyristoyl-*sn*-glycero-3-phospho-choline (DMPC) [21–23]. These systems exhibit disk-like, elongated (ribbon or wormlike micelle), or porous (vesicle or lamellar) aggregates, depending on composition, and have in common the coexistence of a flat bilayer region rich in the long-chain lipid and an edge region preferentially occupied by the short-chain lipid. Such structures are not found at equilibrium among single-component DMPC aggregates in solution, where the line tension drives the system to minimize edge lengths either by fusing bilayer fragments into extended sheets or by curving fragments into closed-shell vesicles. The stability of disk, ribbon, or pore edges in the DMPC/DHPC mixtures indicates that the line tension – the excess free energy per unit length of the edge – is negligible, a result of the line activity of DHPC. The similarity in phase behavior between the simple mixed lipid system (DMPC/DHPC) and the antimicrobial peptide incorporated lipid system (DMPC/PG-1) with substantial biological importance suggests that the structural formation by the two may be driven by the same underlying principle.

The small size, apparent simplicity, and biophysical interest of PG-1 have motivated a number of atomistic simulation studies, recently reviewed [24], aimed at understanding the behavior of PG-1 within the lipid environment. Several simulation studies have been published on the interactions of PG-1 with lipid membranes [25–28]. Langham et al. [27] performed simulations of PG-1 with sodium-dodecyl-sulfate (SDS) and dodecyl-phospho-choline (DPC) micelles that were chosen to model the bacterial and mammalian membranes, respectively. They found a clear difference between the behavior of SDS versus DPC, which implies distinct mechanisms of interaction for PG-1 with bacterial and mammalian membranes. Bolintineanu et al. [29] screened several PG-1 mutants by molecular dynamics simulations in micelle environments, trying to correlate the toxicity of those molecules to their physicochemical properties such as interaction energies and radius of gyration. Jang et al. [30] simulated the interactions of PG-1 with model membrane bilayers consisting of either palmitoyl-oleoylphosphatidyl-choline (POPC) lipids to mimic mammalian membranes or mixed POPC/POPG lipids to mimic bacterial membranes (POPG, or palmitoyl-oleoyl-phosphatidylglycerol, is a negatively charged lipid). They found that the PG-1 molecules bind more strongly to the model bacterial membrane than to the model mammalian membrane because of electrostatic interactions. Kandasamy and Larson performed MD simulations for the interactions of PG-1 with model lipid bilayers of different hydrophobic widths [31]. They showed that PG-1 possessed diverse binding modes in the trans-membrane orientation. They also showed that the membrane disruption was weaker for membranes composed of shorter lipids, and that the assembly of a bilayer in the presence of PG-1 led to a bilayer with a pore stabilized by a transmembrane peptide. The tilting behavior of PG-1 embedded in bilayers of different thickness has been explored in great detail using umbrella sampling calculations by Rui and Im [32] which led to a reinterpretation of NMR results that had originally indicated a large discrepancy between simulation and experiment regarding the tilt angle. Using a structure derived from NMR results [33], Langham et al. [34] modeled octameric PG-1 pores in a barrel-stave arrangement; however, NMR evidence of close headgroup–backbone interactions [35] brought this model into question. Jang, Nussinov, Lal and coworkers simulated PG-1 pores stabilized by eight PG-1 monomers [36]. They found little difference between the oligomeric structures in zwitterionic lipid bilayers and anionic lipid bilayers [36]. Members of the same team subsequently reported MD simulations for PG-1 pores formed by 10 monomers in anionic dioleoylphosphatidylserine/dioleoylphosphatidylethanolamine lipid bilayers showing that these gave better fits to pore sizes determined by AFM [37].

In this work, we present the structural formation in mixed DMPC/PG-1 systems revealed via AFM, and results of full atomistic and coarse-grained molecular dynamics simulations on the perturbation of the lipid bilayer edge by PG-1 molecules. A ribbon geometry is used in the atomistic simulations to mimic the wormlike micelles observed in AFM experiments. The geometry also provides simplicity to analyze the energetics of the edge under periodic boundary conditions [22,38].

Our findings suggest that the lytic effect of PG-1 should not be cast merely as a static picture of the induction of pore structure, but should rather be viewed as a dynamic picture of structural transformations adopted by the lipid–peptide mixture depending on the relative ratio of the two species.

2. Material and methods

2.1. Material

DMPC was purchased from Avanti Polar Lipids, Inc. (Alabaster, AL) and used without further purification. High-grade mica was purchased from Ted Pella, Inc. (Redding, CA). Ultrapure water (resistivity > 18 MΩ cm) was obtained with a MilliQ (Millipore, Bedford, MA) system. Dulbecco's phosphate-buffered saline (D-PBS), without calcium and magnesium (Invitrogen Co., Carlsbad, CA), was used as the superphase for all the experiments. PG-1 was synthesized in-house; the synthesis of the peptide has been described elsewhere [40].

2.2. Experimental methods

The interaction of bilayer patches and PG-1 was studied as follows: Prior to the experiment, the fluid cell was flushed with MilliQ water. (1) Bilayer patches were deposited on the mica surface by vesicle rupture method. (2) After vesicle injection, excess vesicles were purged with buffer solution and AFM images were obtained. (3) PG-1 solution was injected into the superphase and AFM images were taken to record the height profile of the system (see Fig. 1).

Large unilamellar vesicles were prepared via the freeze–thaw extrusion method [40]. The lipid, dissolved in chloroform, was dried to a thin film under a stream of nitrogen and was left overnight in vacuum for the solvent to completely evaporate. The lipid film was then hydrated with water and vortexed at 40 °C for 30 min. A typical concentration used during vesicle preparation was 2 mg/mL. After six

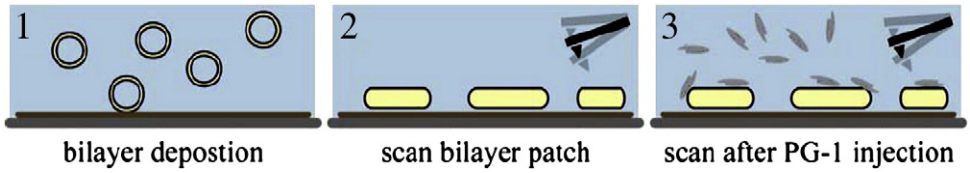

Fig. 1. Experimental protocol for AFM imaging: 1. Formation of lipid bilayer patches via vesicle rupture on mica surface; 2. Imaging bilayer patches after flushing unattached vesicles; 3. Scanning morphology and topology of bilayer patches after the introduction of PG-1.

freeze–thaw cycles, the suspension was extruded through the pores of a polycarbonate membrane (100 nm, Avanti Polar Lipids, Inc.). The size distribution of the resulting vesicles was determined by dynamic light scattering using a model PD2000DLS (Precision Detectors, Franklin, MA) instrument and was typically found to have a diameter of 130 ± 28 nm.

Supported bilayers were formed using the vesicle rupture method. All experiments were performed under buffer using a commercial fluid cell (Digital Instruments, Santa Barbara, CA). Mica fixed on a stainless steel disk was freshly cleaved and used as a substrate. The mica was immediately hydrated by the buffer solution. Subsequently, 0.4 mL of a 20 μg/mL vesicle solution with 10 mM $MgCl_2$ (Fisher Scientific, ACS grade) was injected to the sample chamber. After 2 min, whereby self-assembled bilayer patches have been formed, the sample chamber was flushed with buffer to remove excess vesicles in suspension. With this concentration, the area coverage of resultant bilayers was measured to be around 20%. All experiments were conducted at 30 ± 2 °C, a temperature above the critical temperature of DMPC, so that the bilayers were in a fluid state throughout the experiments. Temperature of the bilayer was maintained constant using a heating controller (Veeco Instruments Inc.) throughout the experiment.

Imaging of the unperturbed supported bilayer was then performed in fluid with a MultiMode Nanoscope IIIA Scanning Probe Microscope (Digital Instruments) using tapping mode. Cantilevers with oxide-sharpened silicon nitride tips (Digital Instruments), with a nominal spring constant of 0.32 N/m were used in tapping mode with a 160-μm scanner (type J). The drive frequency was between 8–9 kHz, and the drive amplitude was between 0.25 V and 0.5 V, which corresponded to 5–10 nm. The setpoint was usually between 0.8 and 0.9 of the free amplitude in our experiments. Minimized tapping force was applied during scan to prevent membrane damage and possible artifacts. Typical scan rate of 1 Hz at a resolution of 256–-512 pixels/line was used. Images shown were subjected to a first-order plane-fitting procedure to compensate for sample tilt, and, if necessary, to a zeroth-order flattening. The height of the bilayer was obtained by analyzing the distribution of surface height over a scan (bearing analysis) or the line section of a scan, depending on the nature and the quality of the image. The area of the bilayer was estimated by counting the number of pixels above a certain threshold value determined by analyzing the distribution of surface height over a scan.

After imaging the unperturbed bilayer patches, PG-1 solution of known bulk concentration (C_b) was injected to fully exchange the superphase. A stock PG-1 (1.0 mg/mL) solution was prepared by dissolving the peptide in ultra-pure water with 0.01% glacial acetic acid to prevent aggregation, and then further diluted to the desired concentration C_b in buffer. An AMP solution of known concentration, C_b, was injected into the fluid cell to fully exchange the superphase.

Two types of AFM measurement were carried out, namely the concentration study and the time-lapse study. In a concentration study, the peptide solution was allowed to equilibrate with the bilayers for an hour, after which structural changes of the same bilayer patch were monitored. This procedure was repeated with increasing C_b to assess the effect of peptide concentration on membrane structure. C_b was increased by 0.5 μg/mL at a time; this small concentration step was used to ensure that the full range of structural transformations could be captured. During equilibration with the bilayer patches, free peptides in the bulk adsorbed to the bilayer until surface partition equilibrium was reached. Since the bilayer patch coverage on the mica surface was approximately the same in each experiment, the peptide to lipid ratio should be directly proportional to C_b [41]. In addition, since approximately the same amount of lipids was present in each experiment, we expect the time-scale for peptide adsorption and equilibration to be independent of C_b [41]. For example, all the changes induced by PG-1 on fluid DMPC bilayer patches were complete within an hour after peptide injection. This long time scale allowed us to carry out time-lapse study. In a time-lapse study, imaging commenced immediately after PG-1 injection, and changes in the structure due to the various states of peptide association were successfully observed.

2.3. Simulation methods

The molecular dynamics simulations were carried out using GROMACS [42–44]. Most simulations were performed on a Linux cluster of Dual-Core AMD Opteron Processor. The VMD package [45] was used for visualization and molecular graphics. The systems investigated are listed in Table 1.

For atomistic ribbon and ribbon/peptide simulations, the starting configuration was taken from the endpoint of a 183-DMPC ribbon system that had been fully equilibrated [38]. The X and Y dimensions of the simulation box were expanded to ~9 nm and ~15 nm, with the Z dimension (along the ribbon edge) fixed at 6.14 nm, to reduce electrostatic interactions between periodic images of the peptides that are inserted into the ribbon later. The empty spaces in the simulation box were filled with water using the genbox utility of GROMACS. The expanded system was then relaxed for 8 ns. Data for the first system (AT-1), a single-component DMPC ribbon, were collected from the endpoint of the 8-ns simulation. Meanwhile, the last frame of the 8-ns simulation was adapted as a template for peptide insertion. Four ribbon systems with PG-1 embedded were investigated. In passing, we note that the two beta-strands of PG-1 stabilized by the disulfide bonds are quite robust, so a vector can be assigned to represent the molecule's orientation. In the beginning, all the peptides inserted to the ribbons are roughly parallel to the normal of the flat part of the ribbons. For the second system, AT-2, a few lipids are removed from both edges of the ribbon to create one hole in each edge. Two peptides were then inserted into the two holes separately, but in a parallel fashion. For the third system, AT-3, two holes were created in each edge of the ribbon. Four peptides were then inserted into the four holes separately in a parallel fashion. The fourth system, AT-4, is

Table 1
Atomistic simulations. Line tension is calculated according to Eq. (1).

System code	System information	Line tension	Duration
AT-1	183 DMPC, 20631 H_2O	37.2 pN	40 ns
AT-2	166 DMPC, 2 PG-1 at edge, 16182 H_2O	38.6 pN	40 ns
AT-3	165 DMPC, 4 PG-1 at edge, 20479 H_2O	19.6 pN	60 ns
AT-4	165 DMPC, 4 PG-1 at edge(anti), 20479 H_2O	13.5 pN	60 ns
AT-5	165 DMPC/4 PG-1 in bulk, 20479 H_2O	65.1 pN	48 ns

similar to the third system except that two peptides inserted into the same edge were roughly anti-parallel to each other. For the fifth system, AT-5, lipids were removed from the flat part of the ribbon to create four holes that accommodate four peptides parallel to each other. System AT-1 contains 183 lipids and 20631 waters. Na^+ and Cl^- ions were added to the lipid/peptide systems for charge-balancing and bringing the system to an ionic strength that is physiologically relevant. The combination of protein OPLS-AA (All Atom) forcefield [46] with united atom lipid forcefield of [47] was used as suggested in reference [48]. The TIP3P water model [49] was used for all simulations. The Berendsen thermostat and barostat [42] were used to maintain a constant temperature of 323 K (with time constant 0.1 ps) and constant 1 bar pressure (with time constant 0.1 ps assuming a compressibility of 4.5×10^{-5} bar) in the X and Y directions, perpendicular to the edge. The box dimension along the ribbon axis was fixed. The particle-mesh Ewald method for electrostatic forces calculated during the MD step [50]. The integration time step was 2 fs, and bond distances were kept constant during MD steps through the SETTLE [51] and LINCS [52] algorithms. The positioning and dynamics of lipids close to the edge are evident from Fig. 2.

Line tension was calculated from the anisotropy of pressure between the main axis along the ribbon edge and the perpendicular axes. As shown in Ref. [22], the line tension Λ in our setup can be calculated in terms of the elements of the pressure tensor P_{xx}, P_{yy} and P_{zz} and the box length L_x and L_y,

$$\Lambda = \frac{1}{2}L_xL_y\left[\frac{1}{2}\left(P_{xx}+P_{yy}\right)-P_{zz}\right]. \quad (1)$$

Here the brackets denote an average over the course of the simulations. No surface tension term appears in this equation because the area of the bilayer ribbon is not constrained by the box dimensions; the bilayer can therefore be considered to be at zero surface tension.

To create random mixtures as initial configurations, PG-1 molecules were first placed, with random orientations at random locations, in a simulation box of size 6.8×6.8×6.8 nm. 128 DMPC lipids were randomly placed in the box as well. The box was then solvated with water and salt ions were added to maintain the charge neutrality of the systems. Before starting long MD simulations, energy minimizations were done to remove bad contacts in the created random mixtures and 1 ns relaxation was implemented with an isotropic pressure coupling scheme, at 300 K, to reduce the internal stresses. The last frames of the relaxation processes were picked as the inputs for conventional MD simulations. To allow the systems to evolve into their optimal states, anisotropic pressure coupling was applied, with the box shape constrained to be orthorhombic. After 80 ns of simulation, the resulting structure was heated with a linear temperature ramp to 500 K over 10 ns, then quenched over 10 ns back to 300 K over 10 ns. The annealed structure was then simulated by conventional MD for an additional 150 ns.

3. Results

3.1. Experimental results

A typical DMPC bilayer patch is shown in Fig. 3A. It exhibited a round contour and a flat lamellar region ranging from 0.1 to a few microns in diameter. Line scans revealed that these patches were 4.4 ± 0.2 nm in height when measured from the bare mica surface. A range of different structural transformations was observed when PG-1 with increasing concentration, C_b, was added to DMPC bilayer patches (Figs. 3 and 4). At $0<C_b<1.5$ μg/mL, no changes in the structure were observed as the bilayer patches remained round and smooth (data not shown, refer to Fig. 3A). However, even at this low concentration, the rigidity of the bilayer was found to be higher in the presence of PG-1 as the AFM tip could trace the patch better, and with less perturbation to the patch shape during lateral scanning. Thus, PG-1 was most definitely associated with the bilayer patches, even though its association did not induce detectable morphological or topological changes. At $1.5<C_b<2$ μg/mL, edge destabilization of the bilayer patches was observed while the lamellar region of the bilayer remained intact, suggesting that the bilayer edge was more susceptible to PG-1 disruption. The fluid bilayer edge became rugged and did not relax back to the round contour with time (Fig. 3B). At $2<C_b<4$ μg/mL (Fig. 4 panels A2, A3, A4, B2, B3, and B4), the edge destabilization was progressively more significant with increasing C_b. In addition, surface defects in the lamellar region were also found, with the number density as well as the size increasing with higher C_b. At $C_b\sim2$ μg/mL, the sparse surface defects appeared, in time-lapse AFM

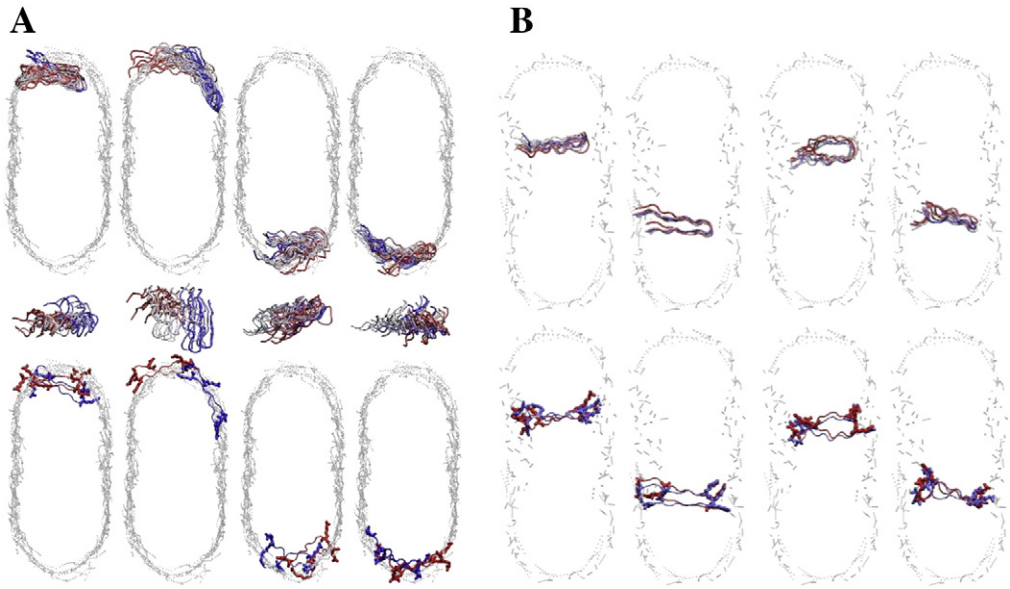

Fig. 2. (A) Trajectories of Protegrin-1 molecules of an 80-ns simulation, for the ribbon that consists of four parallel Protegrin-1 molecules. Beginning of the trajectory is in red, the middle in white, and the end is in blue. The phosphorus atoms in lipid head groups as gray dots visualize the shape of the ribbon. The width of the ribbon, distance from bottom gray dots to top gray dots in the figure, is about 9.5 nm. Lower panel includes initial and final snapshots only, highlighting positions of arginine sidechains. (B) As 2a, but for peptides embedded in "bulk"-like region of the ribbon.

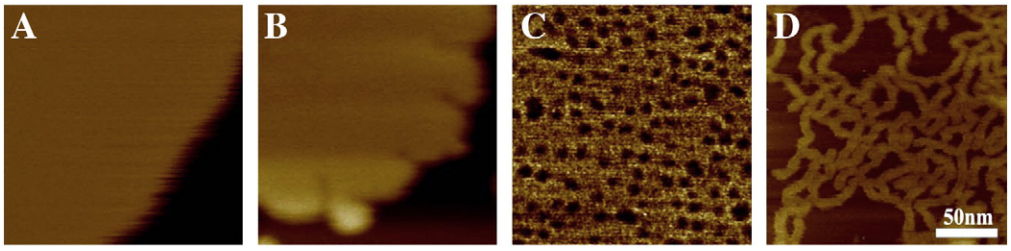

Fig. 3. Atomic force microscopy image of equilibrium structure in DMPC lipid bilayer patch incubated with the increasing concentrations of PG-1 solution on a mica substrate (from A to D). The color scheme shows higher structure with lighter color. (A) Without PG-1, line-tension of a unperturbed liquid lipid bilayer patch maintain a smooth edge contour (B) With the perturbation of PG-1 at low concentration, bilayer contours are extended and stable over time, suggesting line tension is lowered with the incorporation of PG-1 at the edge of the bilayer (C) With further increase of PG-1 content in the bulk, pore formation was observed. While the size of PG-1 molecule is much smaller than the dimension of these pores (~9 nm in diameter), the PG-1 molecules are believed to aggregate in order to induce pore formation (D). At higher concentrations of PG-1, wormlike micelle formation was observed transforming the entire bilayer into a structure with characteristics width of ~7 nm and a much reduced thickness. The rich morphologies of structural transformation in the lipid/PG-1 mixture are reminiscent of phase behavior of DMPC/DHPC mixture, in which DHPC acts as line-active agent to lower line tension.

imaging, to be laterally diffusive within the bilayer patch, and the depth of the defects was measured to be approximately 1–2 nm (Fig. 4, panels A2 and B2). However, the depth measured was resolution-limited by the large AFM tip size (~10 nm radius of curvature) and could not be fully resolved. As the lateral size of the defects increased with increasing C_b, the defects were found to span the entire depth of the bilayer, suggesting that these structures were pores in the bilayer. The structural transformation at the edge of the bilayer patch as well as the porous bilayer interior continued to evolve with increasing C_b. Finally, at $C_b > 4$ μg/mL (see, for example, Fig. 4, panels A5 and B5) wormlike structures were found throughout the bilayer patch. Radial distribution in a Fourier spectrum of these wormlike structures (data not shown) revealed a characteristic width of ~9 nm. The average thickness of the structure was 2.6 ± 0.3 nm from the mica surface, greatly reduced from the original thickness of 4.4 ± 0.2 nm for an unperturbed DMPC bilayer. The wormlike structures persisted to even much higher C_b, representing the final structural transformation observed in the system. At PG-1 concentrations over 20 μg/mL, these structures became easily detachable from the mica surface when scanned by the AFM tip. An AFM time-lapse movie can be found in the Supplemental material, showing the gradual thinning of the bilayer as well as the lateral expansion during the PG-1 induced membrane disruption process. The high-resolution image (Fig. 4 B5) revealed that the bilayer thinning was a process of transforming bilayer into wormlike structures during the disruption.

3.2. Simulation results

Ideally, a molecular dynamics trajectory would be carried out long enough for a peptide to reach the same free energy minimum structure irrespective of starting conditions. In the present case, the slowness of translational diffusion of the peptide (among other degrees of freedom) prevented the direct assessment of the relative stability of PG-1 embedded in flat and rim environments of a bilayer ribbon. Indirect evidence drawn from the effects of PG-1 presence and placement on edge line tension, and structures formed during unbiased assembly of PG-1 containing lipid bilayers provide consistent support for a mechanism of PG-1 action as a line-active agent at the bilayer edge.

3.2.1. Positioning of PG-1 molecules with respect to bilayer edge

The position as well as orientation of PG-1 has been monitored in the course of the atomistic simulations. Snapshots of DMPC ribbons with four PG-1 molecules at the edge are shown in Fig. 5. The PG-1 molecules span the bilayer with the arginines associated with the lipid headgroups and the hydrophobic core associated with the hydrocarbon chains of lipids (Fig. 5B). In most of the cases, arginines at the terminals and at the turn regions are associated with the headgroups of the lipids that approach the edge from opposite leaflets, respectively. This resulted from electrostatic interactions between the arginines and the lipid headgroups. The arginines at the N-terminal

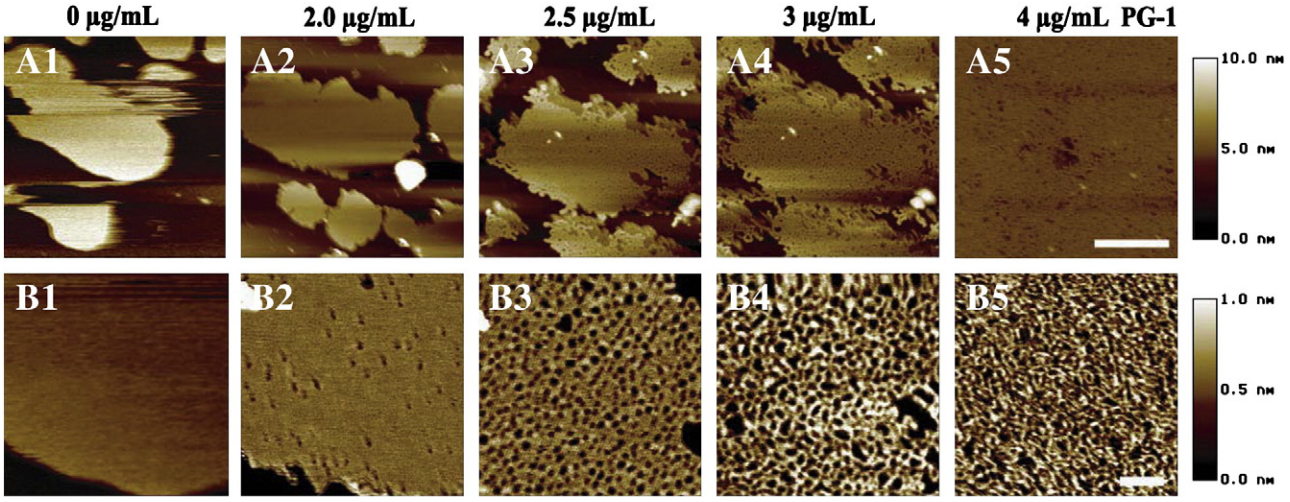

Fig. 4. Atomic force microscopy images of structural transformation with increasing concentration of PG-1. Pore formation was observed at $C_b > 2$ μg/mL, which became denser in number and larger in size with increasing concentration of PG-1 until the formation of wormlike micelles at ~4 μg/mL.

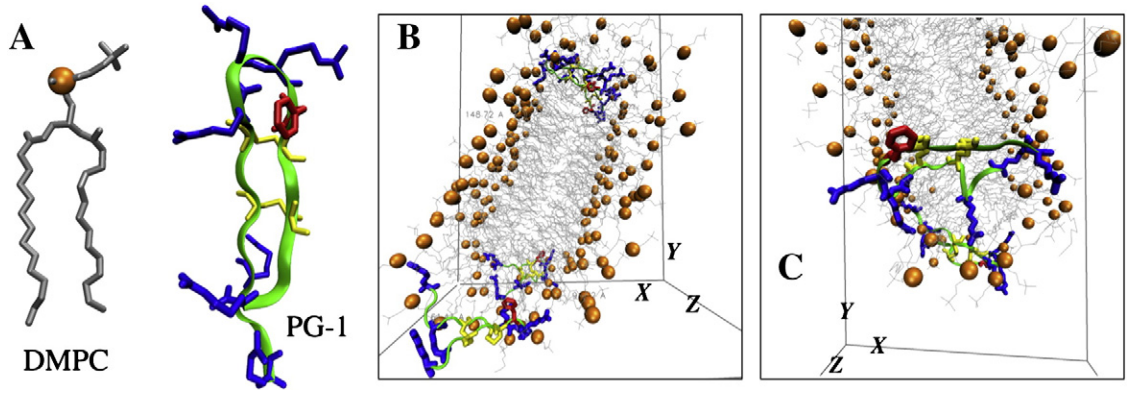

Fig. 5. Shown from left to right are: (A) the structure of the DMPC lipid and the PG-1 peptide, (B) perspective views of the snapshots of atomistic simulation for system AT-3 and (C) system AT-4. The lipids are represented by gray sticks except the phosphorus atoms that are highlighted into orange spheres. The backbones of the PG-1 are represented by green ribbons. The cysteine bridges are represented by yellow sticks and the arginines by blue sticks. The phenylalanines at the turn region are visualized in red, to give a sense of the orientation of the PG-1. It can be seen in (B) and (C) that the arginines at the terminals and the turn region bind to the headgroups of the lipids that approach the edge from opposite leaflets, respectively. The PG-1 in the foreground of (C) is an example that explains why these molecules can stabilize the bilayers edge — the flexible terminal region can easily adjust to curved environment at the edge and thus seal the edge. The arginines in that particular PG-1 pose a neat semicircle arrangement that is almost a perfect fit for the edge.

of the PG-1 molecules are exceptionally flexible, allowing the molecule as a whole to fit to a range of curvatures present at the bilayer edge. In a single-component DMPC ribbon, in order to shield the hydrophobic tails from water, lipids near and at the edge have to bend and rotate about the bilayer normal. The curved environment of the edge is not natural to DMPC, as it dictates an area per headgroup that is larger than in the unperturbed bilayer, so that non-zero line tension arises. With PG-1 molecules embedded in the edge, however, the PG-1 molecules stabilize the curvature by pulling lipid headgroups from opposite leaflets toward each other, since the natural length of the PG-1 is less than the thickness of the DMPC bilayer. When doing so, however, PG-1's own hydrophobic part was partially exposed to water. Our observations indicate that lipids not being displaced from the edge help shield PG-1's hydrophobic part from water. An occurrence is found that the peptide hairpin turn region and the terminals of PG-1 bend toward to the surface of the bilayer edge (as illustrated in Fig. 5C). The arginines in that particular PG-1 arrange into a neat semicircle that nicely fits the curved edge. It has been proposed that PG-1 could stay in a flat bilayer with different binding modes characterized by different tilting angles [53]. Our results further showed that PG-1 embedded at the edge of the DMPC ribbon were relatively free to rotate (Fig. 2A), while peptides embedded in the bulk show much lower orientation fluctuations (Fig. 2B) over 80 ns of simulation. Simulations were initiated without close peptide–peptide contacts and remained separated throughout the simulation; no conclusions could be drawn from the simulations regarding the formation of either parallel or anti-parallel dimers.

3.2.2. Lowering membrane line tension by PG-1

With one PG-1 molecule embedded in each edge (at a spacing of 1 peptide per 6.12 nm of edge length), the ribbon yields approximately the same line tension in comparison to a single-component DMPC ribbon (~37–38 pN), as demonstrated by data in Table 1. Ribbons with two parallel or anti-parallel PG-1 molecules embedded in each edge (at an average spacing of 1 peptide per 3.06 nm of edge length) yield line tensions lower by 47% and 64%. To distinguish actual stabilization of the edge from any non-specific effects of including the highly charged peptides in an anisotropic box, control simulations were performed in which the peptides were embedded in the flat "bulk" portion of the bilayer ribbon rather than at the edge — these simulations yielded increases in calculated line tensions. While trajectory times were insufficient to observe PG-1 moving towards or away from the edge, the decrease in line tension is evidence that the peptide is a line-active agent, which would necessarily indicate that it would be enriched at the edge at equilibrium.

The line tension of the DMPC ribbons studied at present with a few peptides at the edge does not drop to zero, but remains high enough (between 13 and 20 pN, or ~3–5 k_BT per nm of edge) to suppress the development of such edge instabilities as shown in Fig. 3. Given that at the highest line density studied, a significant amount of DMPC surface remains exposed at the rim, it is reasonable to conjecture that a higher peptide line density could be achieved (either by removal of DMPC – shortening the edge – or addition of PG-1 at constant edge length) and would yield a further lowering of line tension. Further studies at higher line density would be needed to determine whether in this model a truly stable (zero line-tension) edge can be achieved, as was found in DHPC/DMPC ribbons [54].

3.2.3. Unbiased assembly results

As the migration of PG-1 among different membrane environments is slow on the simulation timescale, simulations were performed of the self-assembly of PG-1 containing bilayers from isotropic, random mixtures of peptide, lipid, and water. While the strongly irreversible nature of these simulations means that the structures formed may not be fully equilibrated, the procedure has the possibility of yielding structures that would not otherwise be predicted. In a control run, where PG-1 molecules were absent, a random mixture of DMPC in water evolved into a bilayer after 90 ns simulation time. Mixtures containing 6, 8, or 12 PG-1 yielded lipid aggregates with complex topologies, in which PG-1 placement could not be easily analyzed. The mixture containing 4 PG-1 molecules evolved into a structure containing a line defect reminiscent of a seam between two bilayer ribbon edges. The defect appeared stable at the end of an 80-ns simulation. Fig. 6A, B and C shows the snapshots at 10, 40 and 80 ns simulation times, respectively, at 300 K. Two PG-1 molecules were co-localized with the defect. To check whether the defect would survive perturbations, one round of heating and cooling was carried out at constant volume. The temperature was first raised linearly from 300 K to 500 K over 10 ns run, which partially smeared the defect in the end of the simulation (Fig. 6D). Over the next 10 ns of the trajectory, the temperature was dropped linearly from 500 K to 300 K (Fig. 6E), and the system was equilibrated for a further 150 ns (Fig. 6F–H). During heating and cooling, one of the peptides associated with the defect (depicted in yellow) moved into a partially trans-bilayer position while the edge defect became a hydrophilic pore defect, containing solvent and lined with lipid headgroups. The trans-bilayer peptide, highlighted in Fig. 7, in fact occupies a

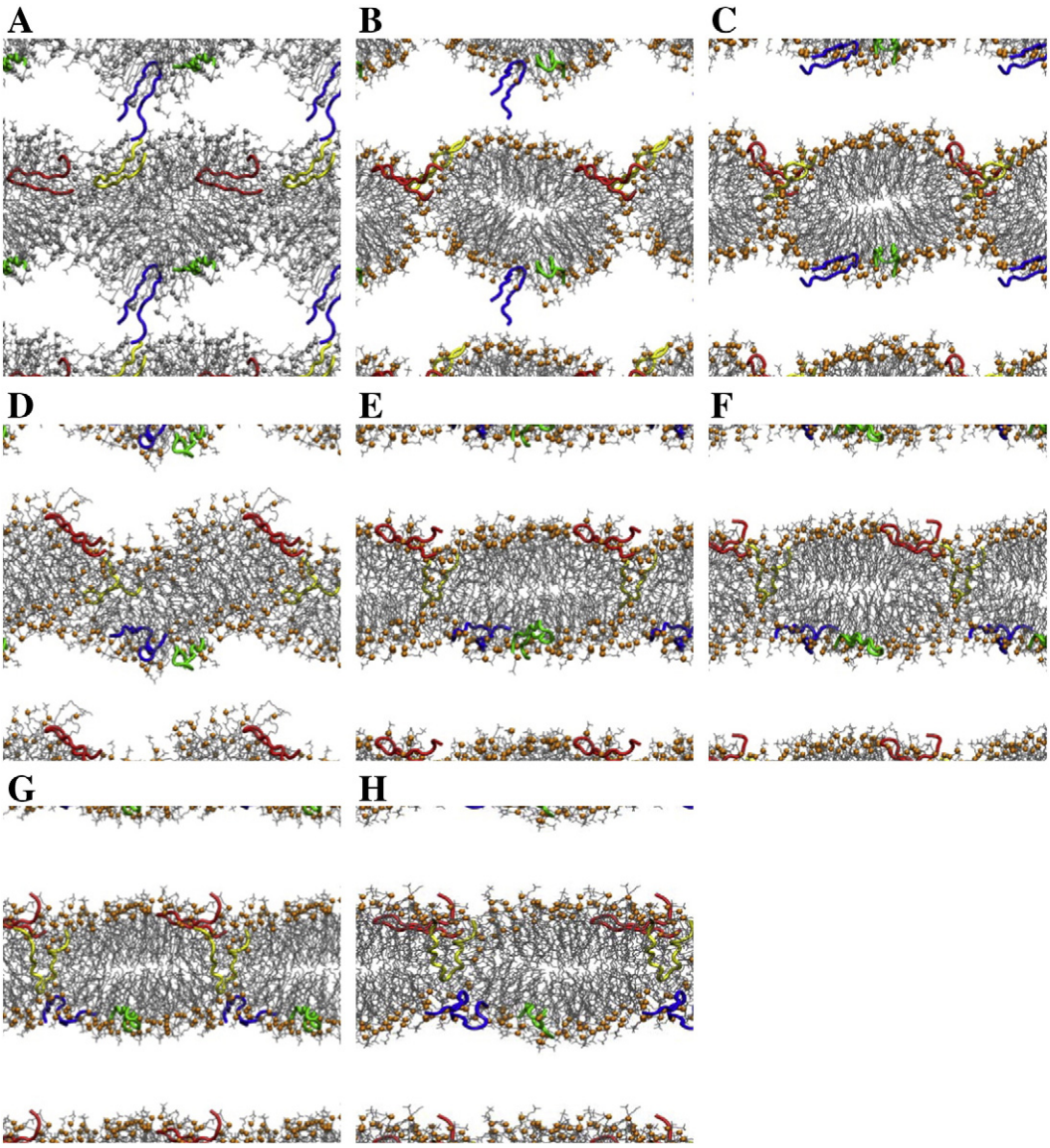

Fig. 6. Snapshots from assembly, heating and cooling of initial random mixture of 128 DMPC, 4 PG-1 peptides, 5227 waters, 9 Na^+ and 33 Cl^- ions: (A) 10 ns, (B) 40 ns, (C) 80 ns, all at 300 K; (D) at the end of another 10 ns run during which the temperature was raised from 300 K to 500 K; (E) another 10 ns run during which the temperature was lowered from 500 K to 300 K; and extended equilibrations at 300 K after that: (F) 50 ns, (G) 100 ns, and (H) 150 ns. The total simulation time was 250 ns.

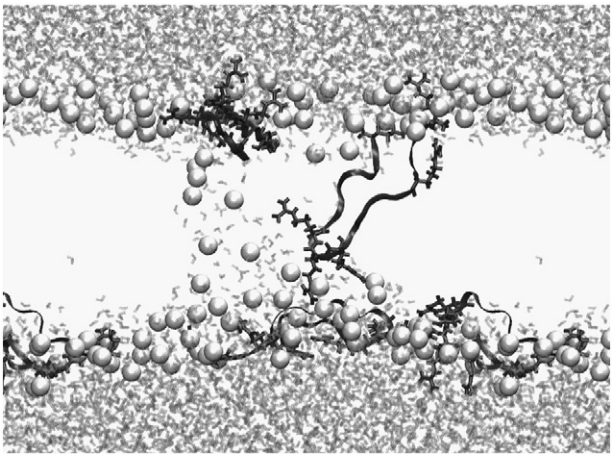

Fig. 7. Side-view of pore-containing bilayer from endpoint of DMPC/PG-1 self assembly run. DMPC position is represented by phosphorus atom site only (large spheres); water represented as gray sticks, PG-1 with dark ribbon backbones with only Arg sidechains visualized.

conformation similar to those observed at bilayer ribbon edges, extending from a flat surface of the bilayer to the curved opening of the pore, with arginine sidechains interacting with solvent and headgroups.

4. Discussion

Definitive demonstration of the mode of peptide disruption of a bilayer is difficult both for experiment and even within a simulation model, especially as a single peptide may exhibit more than one mode of interaction with the bilayer. The current simulations of bilayer ribbons showed considerable variability in the details of peptide placement near the edge, with some remaining parallel to the bilayer normal, embedded firmly in the hydrophobic tail region, and others staying closer to the interface and shifting around the rim. In a simulation of 4 PG-1 and 128 DMPC self-assembling into a bilayer from a random mixture, two of the PG-1 were found at edge-like line defect site. After a cycle of heating and cooling, lipids and peptides rearranged, leading to a small hydrophilic pore associated with one transmembrane peptide and two surface-associated peptides. In the

present work, the observation that the line tension of a bilayer ribbon's edges is reduced when PG-1 is placed near the edge provides evidence that this peptide behaves as a line-active agent with a greater affinity for the edge than for the intact bilayer.

It is intriguing the rich structural transformations in Figs. 3 and 4 can be the results from the interaction of two rather simple molecules: a phospholipid and an 18-residue AMP. Here, we discuss the driving force and give a molecular interpretation of these PG-1 induced structures (Fig. 8). Understanding the driving force and the energetics for the bilayer structural transformation induced by PG-1 might help shed light on the mechanism of how other antimicrobial peptides work.

4.1. PG-1 preferentially binds to locations of high curvature, lowering the line tension of the bilayer edge

At a low C_b, instability begins at the edge of the lipid bilayer patch, which does not relax to a smooth contour over time. Although an edge like the one in a bilayer patch does not exist in the usual cell membrane geometry and the peptide exerts its activity by binding to the lamellar portion of the membrane, the edge instability nonetheless reveals an invaluable physical property of PG-1. Before we can understand why the edge does not relax spontaneously, we need to discuss the origin of line tension in the bilayer patch.

To prevent direct exposure of the hydrocarbon chains to the aqueous environment in a pure lipid bilayer patch, lipid molecules self-assemble to form a highly curved cap at the edge of the lipid bilayer (Fig. 8A). With lipid having neutral or positive spontaneous curvature, their alignment in the cap region can induce steric stress due to tail interactions. As a result, it is energetically less favorable for these lipid molecules to stay at the edge than in the lamellar core of the patch, and the penalty comes in terms of a line energy, a 1D equivalent of the more familiar surface energy for a 2D surface. Many factors, including steric effects between lipids, the spontaneous curvature of the lipids, and the difference in the number of neighboring molecules, contribute to this line energy. Line tension acts to minimize the line energy, by reducing the length of the border. A fluid supported bilayer patch has a minimized edge contour due to the action of line-tension. The energy-costly edge can be eliminated by assembling into other structures such as the closed structure of vesicles, or reduced by adsorbing line-active agents at the border [55,56]. Free PG-1, when dissolved in the bulk, partitions between the bilayer surface, the bilayer edge, and the bulk to an equilibrium balance of chemical potentials. The initial observation of edge instability suggests that PG-1 does adsorb from the bulk to the edge even at a small bulk PG-1 concentration. By preferentially adsorbing to the edge, PG-1 molecules lower the line energy and reduce the line tension (Fig. 8B), giving rise to a rugged and more extended edge that does not relax to a minimized contour (see Fig. 3B). Our results therefore indicate that PG-1 is line-active.

Indeed, the concentration dependent results of our study are in line with other observations involving other line-active agents. Like detergents, which lower the tension of water surface (2D), these line-active agents can be considered as detergent that is active in 1D. As measured in detergent–membrane systems, detergent molecules are line-active and preferentially bind to the edge of the bilayer to lower line energy [56,57]. The reduction in line tension of the lipid patch is analogous to the Gibbs adsorption isotherm when the amount of adsorbed detergent is small. As the amount of detergent is increased to a certain critical concentration, C_b^*, the line tension cannot be further reduced as adsorption at the edge has reached saturation. Detergent molecules begin to bind to the lamellar region of the bilayer after saturating the edge of the bilayer. Ideally, adsorption of detergent molecules to the lamellar surface does not contribute to the line tension. In our experiments, PG-1 molecules act like one-dimensional detergents lowering the line tension of bilayer edges.

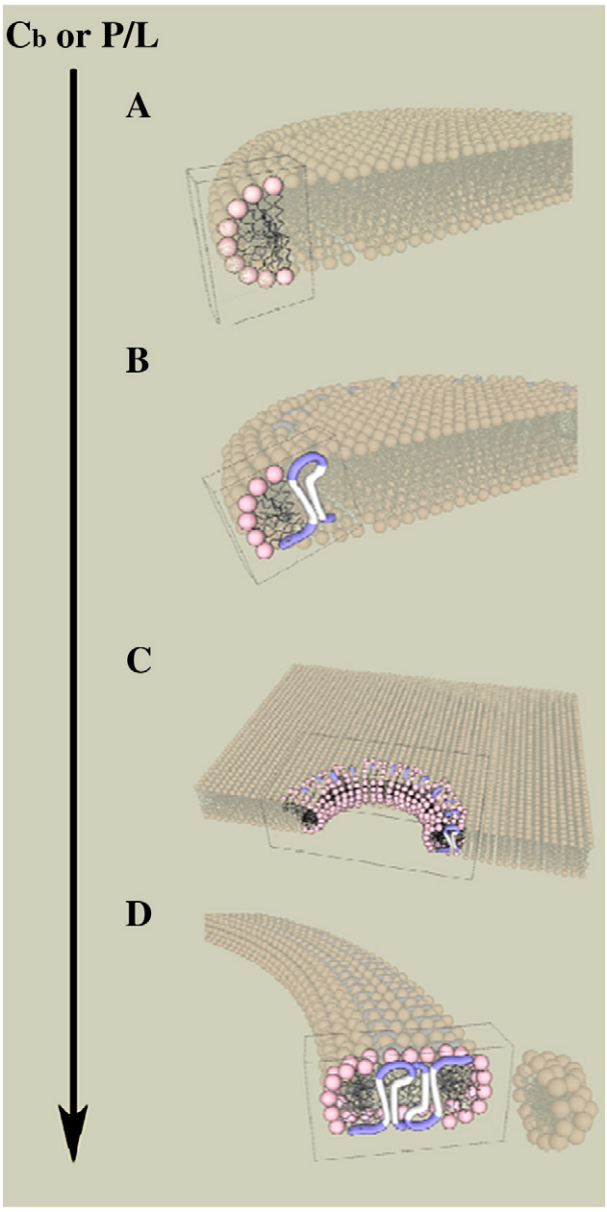

Fig. 8. Model of line activity induced structural transformations. The schematics provide a molecular view of structural transformations adopted by the lipid–peptide mixture as a function of the relative ratio of the two species. Depending on the concentration of PG-1 (C_b), and therefore the peptide to lipid ratio (P/L), PG-1 and lipid assemble into various structures in the course of membrane disruption. A PG-1 molecule is represented by a hairpin shape molecule with a hydrophobic core (white) flanked by cationic groups (blue). A DMPC lipid molecule is represented by a zwitterionic headgroup (pink) and hydrophobic tails. (A) A lipid bilayer edge with steric stress contributing to its line energy is unfavorable. (B) PG-1 binds to a bilayer edge and lowers the line tension of the bilayer, forming a fundamental unit of the lipid–peptide complex which stabilizes the lipids at the edge. (C) PG-1 not only binds to the curved edge, but also creates local curvature by forming pores. However, pore formation only represents an intermediate step of the structural transformation. (D) At higher P/L, the stable units of the lipid–peptide complex combine to form wormlike micelles, a thinner and elongated structure. The relative orientation in the peptide dimer is for illustration only. Figures are not to scale; refer to the text for detailed explanations.

The observed edge instability corresponds to the edge adsorption stage at $C_b<C_b^*$ (Fig. 8B); similar undulatory instability at the edge was seen in coarse-grained [22] and atomistic [54] simulations of DMPC/DHPC mixed ribbons beyond a critical fraction of DHPC. With further increase in C_b, the accumulated surface adsorption reaches a critical stage to induce structural transformations, including pore

and wormlike micelle formation in the lamellar region (Fig. 8C and D). At the same time, the extended contour length resulted from these structural transformation acts to lower the density of adsorbed peptides of the edge, which in turn allows for further peptide edge adsorption.

Lowered line tension due to the stabilization of the curved edge state may be observable for other AMP's with different secondary structure. For instance, stabilization of nanometer-sized pores observed in simulations of the alpha helical AMP magainin [58] was similarly attributed to the induction and stabilization of lipid curvature in a "disordered toroidal pore" model, effects that are likely to remain important whether the curvature is associated with the inside edge of a pore or an extended edge.

4.2. Adsorbed peptide can induce local curvature change, giving rise to a rich spectrum of mesophases

At higher C_b, the rich structural transformation observed in the lipid–peptide assembly is reminiscent of a classic amphiphilic system involving a binary mixture of short- and long-chain lipids such as DHPC and DMPC [21–23]. DHPC is a mild detergent with the same headgroup as DMPC, but only six carbons in the two acyl chains (versus 14 in DMPC). DHPC is well-known for its ability to form bicelle structure when mixed with DMPC [21–23]. DHPC is a line-active molecule, and, when mixed with lipids, preferentially occupies the edge in the mixed assembly. The structural transformations observed in the DMPC/DHPC system share strikingly common characteristics with our DMPC/PG-1 system. With increasing ratio of line-active agent (DHPC) vs lipid (DMPC), q, the bilayer undergoes structural transformations from a perforated bilayer, to wormlike micelle formation, and finally to bicelle (disk) and micelle formation. With the incorporation of DHPC at a low q, the DMPC/DHPC binary mixture adopts a porous sheet geometry, with the line-active DHPC collecting around the pore and raising its linear density. Pore size and density also increase with increasing DHPC content. As the DHPC content further increased, flexible wormlike micelles are found to be ribbon-like, rather than cylindrical. Presumably, the edges of these ribbon-like structures are preferentially occupied by DHPC molecules as well [21]. Further increase in DHPC content leads to the formation of bicelles and micelles (Fig. 8 in Ref. [59]). A model representation of DMPC/PG-1 mixtures as a function of PG-1 content is proposed in Fig. 8, which bears great resemblance to the manner of structural changes found in the DMPC/DHPC system. It should be pointed out that the forces that drive DHPC and PG-1 to the edge in their corresponding mixed systems might not be identical: they have different solubility in water and mix with DMPC to a different extent. Nonetheless, the two systems form analogous structures as both DHPC and PG-1 act as line-active agents.

4.3. Molecular structure of wormlike-micelles and pores

While sharing similar mesophases of the DMPC/DHPC system, the DMPC/PG-1 mixture is likely to have different molecular details in the orientation and the spatial arrangement of the two species. We will first discuss the molecular structure of wormlike micelle and pores, and then speculate on the stages in their formation in light of the line-active characteristic of PG-1 in membrane.

At a high enough C_b, the entire planar DMPC bilayer transforms into wormlike micelles with a characteristic width and height, highly differentiated from the lamellar structure of the lipid bilayer. Similar transformation has been observed when PG-1 is added to saturated, unsaturated or cationic lipids, suggesting that wormlike micelle formation is not specific to lipid architecture [60]. The possible molecular model for the formation of pore and wormlike micelles as proposed in Fig. 8 is based on the following: 1) the dimensions of the wormlike structure from our experiments, 2) the dimensions and structures of the peptide and the lipid [19,39,61], 3) the orientations of the peptide and the lipid [62–66], 4) the hydrophobic–hydrophilic interaction between the molecules, and 5) curvature and electrostatic considerations. A DMPC lipid molecule is represented by a zwitterionic headgroup (pink sphere) and hydrophobic tails (black wiggly lines) in Fig. 8A. The peptide forms an anti-parallel β sheet with the strand constrained by two disulfide bonds and joined by a β turn, resembling a hairpin. The central portion of the β sheet in PG-1 is relatively restricted in shape and contains only apolar residues on both surfaces (white) whereas charged residues are clustered in the turn region and at the two terminus (blue) [39]. The disulfide bond has been shown to be essential for PG-1 activity as analogs of PG-1 without disulfide bonds show diminished activity under certain salt conditions, whereas wild type PG-1 molecules are immune to salt effects [67]. Recognizing the importance of the architecture of the two disulfide bonds in PG-1 activity, we represent the peptide by a dumbbell shape with a hydrophobic core (white) flanked by cationic groups (blue) to illustrate the tightly bound disulfide bonds region (Fig. 8B). We assume the peptide drives lipids with a neutral spontaneous curvature to form a stable lipid–peptide unit (Fig. 8B) with higher curvature, and therefore lowering the line tension of bilayer edge. Line tension continues to lower with the formation of lipid–peptide complex, resulting in various molecular structures as in edge adsorption (Fig. 8B), pore formation (Fig. 8C) and wormlike micelles growth (Fig. 8D).

In a pore geometry (Fig. 8C), the formation of an edge follows the two lipid leaflets as they bend towards each other, assembling into a stable structure with minimal exposure of the hydrophobic core to the surrounding aqueous phase. When pore density and pore size increase as the number of lipid–peptide units grows with increasing C_b, pores can encounter one another with their peptide "backbones" facing opposite to each other. As a result, PG-1 can form dimers, and these dimers can be embedded in the center of the wormlike micelle (Fig. 2D). Although a monomer construct for the wormlike micelle is possible, the dimer backbone provides a width that is more commensurate with our AFM measurements, and agrees with NMR studies reporting that a dimeric structure is adopted by PG-1 when bound to lipids [39,68–72], though neither our experimental nor our simulation results can confirm the proposed antiparallel dimeric structure from NMR results. Furthermore, amide proton exchange studies have also suggested the possibility of an association between several dimers [68].

In a wormlike micelle geometry (Fig. 8D), due to the disruption of lipid orientation, the height of the structure is significantly reduced. In our experiments, we have measured a significant decrease in the height of the wormlike structure from the lipid bilayer. In fact, the height of the wormlike micelle is close to that of the long molecular axis of PG-1. The physical dimensions of a PG-1 molecule are ~8 Å wide by ~25 Å long [19], whereas that of a DMPC lipid molecule are ~55 $Å^2$ in the cross-sectional area [61,73] by ~22 Å long [74]. Since the length of the hydrophobic chains of DMPC in the extended conformation is about 14 Å [74], which would give rise to a bilayer with a hydrophobic core diameter of about 28 Å. It would be hard to imagine any lipid bilayer structure could have the much lowered height of 2.6 nm observed in the wormlike micelles, and the observed structure is a logical consequence of the line-active nature of PG-1 and high peptide concentrations. These stabilized extended structures, however, are reminiscent of those observed when *E. coli* cells are exposed to PG-1 where the outer membrane is greatly expanded and thrown into numerous folds (microvilli) that are absent in untreated controls [19].

Our model for wormlike micelles and pores thus agrees with both the geometric parameters of the molecules and our experimental results. In the model (Fig. 8D), hydrophobic tails of DMPC molecules associate with the hydrophobic part of PG-1. The polar headgroups of the lipid molecules form a surface of prolate ellipsoid shield, and

prevent the hydrophobic parts from being exposed to the aqueous environment. Notice that the DMPC molecules are oriented perpendicular to the peptide in the model, forming a semi-cylindrical belt around the hydrophobic surface. This model agrees with extensive solid-state NMR studies, showing that PG-1 inserts at an angle into the membrane and can disorder lipid orientation in zwitterionic phosphatidylcholine bilayers [62–65]. NMR has also shown that PG-1 molecules form oligomeric aggregates that contact both the surface and the hydrophobic center of the PC bilayer [63]. Furthermore, there is close contact between the lipid chains and the peptide [66], and it has been proposed that PG-1 disrupts the DMPC membrane by breaking the extended bilayer into smaller structures, whereby a significant fraction of lipids are located at the edges of the structure with a distribution in lipid orientation [65].

The main driving force for these structural formations lies with the principle of energy minimization, including contributions from the curvature of the resulted structure, and the electrostatics as well as the hydrophilic–hydrophobic interactions between lipid and PG-1 molecules. The zwitterionic or the anionic lipid headgroup associates with the cationic peptide through dipole–charge or charge–charge interactions, while the hydrophobic core of the peptide stabilizes the structure through favorable interactions with the hydrocarbon chains of the lipids. While the hydrophilic part of PG-1 is positively charged, the lipid as well as the associated water molecules would further act as a dielectric shield between repulsive peptides. The screening length in our experiments is on the order of 1 nm, allowing short-range electrostatic interactions to be significant. With the addition of salt, the screening of long range electrostatic repulsions between the charged lipids or peptides would allow a stable aggregation of the lipids and the peptides, resulting in the formation of the wormlike micelle. In an environment without the contribution of salt screening, we have observed from our experiment that membranes containing anionic lipids in a pure water superphase result in structures that are easily detachable by the AFM tip. These results suggest that the long-range electrostatic repulsion between peptides may reduce the overall length of the wormlike micelles.

5. Conclusion

A combination of experimental and simulation results provides evidence that PG-1 behaves as a line-active agent, stabilizing the edge of the DMPC bilayer in analogy to the activity of DHPC in DMPC/DHPC “bicelle” mixtures. In general, direct edge stabilization can be added to the list of proposed mechanisms by which this and similar antimicrobial peptides can disrupt membranes, including formation of small octamer pores [71] and general electrostatic effects [75]. Further simulation work will be necessary to examine at higher line densities of peptides at the edge, which could potentially yield insight into structural changes due to dimerization or other peptide–peptide interaction, and the density of peptides necessary to fully stabilize the edge.

We show that the reduction of line tension by PG-1 can be demonstrated by simulating a DMPC bilayer ribbon with free edges. As demonstrated in the DMPC/DHPC system, line-active agents could induce structural transformation, including pore and wormlike micelle formation. The lytic effect by antimicrobial peptides is usually attributed to the formation of pores in the lipid membrane. These structural transformation mechanisms by line-active agents may therefore be responsible for the stabilization of pore formation and the subsequent membrane disruption by antimicrobial peptides.

Our study helps elucidate the mechanism through which PG-1 stabilizes the edge of lipid bilayers. The PG-1 molecules that are placed to bilayer edge have been found to lower the line tension of the edge. It should be a stage through which more advanced structures of PG-1 assembly emerges when the PG-1 concentration increases. The line tension of the DMPC ribbons studied at present with few peptides in edge does not drop to zero. The line tension of DMPC/DHPC ribbons [54], on the other hand, approaches zero progressively with increasing fraction of the shorter-tail lipids, as demonstrated by our simulations. It is worthwhile to simulate ribbons with more PG-1 molecules placed at the edge next. It is possible that above a threshold in the line density of the peptides, these peptides start to interact with each other and aggregate into an assembly that truly facilitates the growth of the edge. The line tension is expected to be zero when this happens. Also needs to be investigated is the impact of PG-1 mutants to the stability of bilayer edge, in order for us to pin down the uniqueness in PG-1's structure. As mentioned in the Introduction, Langham et al. [28] attempted to correlate toxicity of PG-1 mutants to their physicochemical property such as radius of gyration in aqueous solvent. Directly simulating the behavior of those mutants in bilayer edge will give further insight into the mechanism of line-active role of these mutant peptides.

Supplementary materials related to this article can be found online at doi:10.1016/j.bbamem.2011.11.002.

Acknowledgements

This work was supported in part by the University of Chicago Materials Research Science and Engineering Center program of the National Science Foundation (DMR 0820054) and the NSF grants to K.Y.C.L. (MCB-0920316) and J.T.K (CHE-0616383 and CHE-0911285). T.A.S. is grateful for the support of the James Franck Institute Summer Research Fellowship.

Reference

[1] L.V. Chernomordik, M.M. Kozlov, The protein coat in membrane fusion: lessons from fission, Traffic 3 (2002) 256–267.
[2] S.L. Schmid, Clathrin-coated vesicle formation and protein sorting: an integrated process, Annu. Rev. Biochem. 66 (1997) 511–548.
[3] M.M. Kozlov, Dynamin: possible mechanism of “pinchase” action, Biophys. J. 77 (1999) 604–616.
[4] S.L. Schmid, M.A. McNiven, P.D. Camilli, Dynamin and its partners: a progress report, Curr. Opin. Cell Biol. 10 (1998) 504–512.
[5] M.M. Kozlov, Fission of biological membranes: interplay between dynamin and lipids, Traffic 2 (2001) 51.
[6] U. Seifert, Configurations of fluid membranes and vesicles, Adv. Phys. 46 (1997) 13–137.
[7] N. Sciaky, J. Presley, C. Smith, K.J.M. Zaal, N. Cole, J.E. Moreira, M. Terasaki, E. Siggia, J. Lippincott-Schwartz, Golgi tubule traffic and the effects of Brefeldin A visualized in living cells, J. Cell Biol. 139 (1997) 1137–1155.
[8] J.A. Killian, I. Salemink, M.R.R. de Planque, G. Lindblom, R.E. Koeppe, D.V. Greathouse, Induction of nonbilayer structures in diacylphosphatidylcholine model membranes by transmembrane alpha-helical peptides: importance of hydrophobic mismatch and proposed role of tryptophans, Biochemistry 35 (1996) 1037–1045.
[9] S. May, A. Ben-Shaul, Molecular theory of lipid–protein interaction and the L_{α}–H_{II} transition, Biophys. J. 76 (1999) 751–767.
[10] B. Christensen, J. Fink, R.B. Merrifield, D. Mauzerall, Channel-forming properties of cecropins and related model compounds incorporated into planar lipid membranes, Proc. Natl. Acad. Sci. 85 (1988) 5072–5076.
[11] K. He, S.J. Ludtke, D.L. Worcester, H.W. Huang, Neutron scattering in the plane of membranes: structure of alamethicin pores, Biophys. J. 70 (1996) 2659–2666.
[12] P. Juvvadi, S. Vunnam, R.B. Merrifield, Merrifield, synthetic melittin, its enantio, retro, and retroenantio isomers, and selected chimeric analogs: their antibacterial, hemolytic, and lipid bilayer action, J. Am. Chem. Soc. 118 (1996) 8989–8997.
[13] S.J. Ludtke, K. He, W.T. Heller, T.A. Harroun, L. Yang, H.W. Huang, Membrane pores induced by magainin, Biochemistry 35 (1996) 13723–13728.
[14] K. Matsuzaki, M. Harada, T. Handa, S. Funakoshi, N. Fujii, H. Yajima, K. Miyajima, Magainin 1-induced leakage of entrapped calcein out of negatively-charged lipid vesicles, Biochim. Biophys. Acta (BBA) - Biomembr. 981 (1989) 130–134.
[15] K. Matsuzaki, O. Murase, N. Fujii, K. Miyajima, An antimicrobial peptide, magainin 2, induced rapid flip-flop of phospholipids coupled with pore formation and peptide translocation, Biochemistry 35 (1996) 11361–11368.
[16] A. Mor, P. Nicolas, The NH_2-terminal alpha-helical domain 1–18 of dermaseptin is responsible for antimicrobial activity, J. Biol. Chem. 269 (1994) 1934–1939.
[17] K.L.H. Lam, Y. Ishitsuka, Y. Cheng, K. Chien, A.J. Waring, R.I. Lehrer, K.Y.C. Lee, Mechanism of supported membrane disruption by antimicrobial peptide protegrin-1, J. Phys. Chem. B 110 (2006) 21282–21286.
[18] Y.A. Domanov, P.K.J. Kinnunen, Antimicrobial peptides temporins B and L induce formation of tubular lipid protrusions from supported phospholipid bilayers, Biophys. J. 91 (2006) 4427–4439.

[19] D. Gidalevitz, Y. Ishitsuka, A.S. Muresan, O. Konovalov, A.J. Waring, R.I. Lehrer, K.Y.C. Lee, Interaction of antimicrobial peptide protegrin with biomembranes, Proc. Natl. Acad. Sci. 100 (2003) 6302–6307.
[20] M. Meincken, D.L. Holroyd, M. Rautenbach, Atomic force microscopy study of the effect of antimicrobial peptides on the cell envelope of *Escherichia coli*, Antimicrob. Agents Chemother. 49 (2005) 4085–4092.
[21] M.P. Nieh, V.A. Raghunathan, C.J. Glinka, T.A. Harroun, G. Pabst, J. Katsaras, Magnetically alignable phase of phospholipid "bicelle" mixtures is a chiral nematic made up of wormlike micelles, Langmuir 20 (2004) 7893–7897.
[22] Y. Jiang, J.T. Kindt, Simulations of edge behavior in a mixed-lipid bilayer: fluctuation analysis, J. Chem. Phys. 126 (2007) 045105.
[23] T.A. Harroun, M. Koslowsky, M.P. Nieh, C.F. deLannoy, V.A. Raghunathan, J. Katsaras, Comprehensive examination of mesophases formed by DMPC and DHPC mixtures, Langmuir 21 (2005) 5356–5361.
[24] D.S. Bolintineanu, Y.N. Kaznessis, Computational studies of protegrin antimicrobial peptides: A review, Peptides, 32 188–201.
[25] H. Khandelia, A.A. Langham, Y.N. Kaznessis, Driving engineering of novel antimicrobial peptides from simulations of peptide–micelle interactions, Biochim. Biophys. Acta-Biomembr. 1758 (2006) 1224–1234.
[26] A.A. Langham, H. Khandelia, Y.N. Kaznessis, Simulations of protegrin-1 in sodium dodecylsulfate and dodecylphosphocholine micelles, Biophys. J. 88 (2005) 210a-210a.
[27] A.A. Langham, H. Khandelia, Y.N. Kaznessis, How can a beta-sheet peptide be both a potent antimicrobial and harmfully toxic? Molecular dynamics simulations of protegrin-1 in micelles, Biopolymers 84 (2006) 219–231.
[28] A.A. Langham, H. Khandelia, B. Schuster, A.J. Waring, R.I. Lehrer, Y.N. Kaznessis, Correlation between simulated physicochemical properties and hemolycity of protegrin-like antimicrobial peptides: predicting experimental toxicity, Peptides 29 (2008) 1085–1093.
[29] H. Jang, B. Ma, T.B. Woolf, R. Nussinov, Interaction of protegrin-1 with lipid bilayers: membrane thinning effect, Biophys. J. 91 (2006) 2848–2859.
[30] D.S. Bolintineanu, A.A. Langham, H.T. Davis, Y.N. Kaznessis, Molecular dynamics simulations of three protegrin-type antimicrobial peptides: interplay between charges at the termini, β-sheet structure and amphiphilic interactions, Mol. Simul. 33 (2007) 809–819.
[31] S.K. Kandasamy, R.G. Larson, Binding modes of protegrin-1, a beta-strand antimicrobial peptide, in lipid bilayers, Mol. Simul. 33 (2007) 799–807.
[32] H. Rui, W. Im, Protegrin-1 orientation and physicochemical properties in membrane bilayers studied by potential of mean force calculations, J. Comput. Chem., 31 2859–2867.
[33] R. Mani, J.J. Buffy, A.J. Waring, R.I. Lehrer, M. Hong, Solid-state NMR investigation of the selective disruption of lipid membranes by protegrin-1, Biochemistry 43 (2004) 13839–13848.
[34] A.A. Langham, A.S. Ahmad, Y.N. Kaznessis, On the nature of antimicrobial activity: a model for protegrin-1 pores, J. Am. Chem. Soc. 130 (2008) 4338–4346.
[35] M. Tang, A.J. Waring, M. Hong, Phosphate-mediated arginine insertion into lipid membranes and pore formation by a cationic membrane peptide from solid-state NMR, J. Am. Chem. Soc. 129 (2007) 11438–11446.
[36] H. Jang, B. Ma, R. Lal, R. Nussinov, Models of toxic β-sheet channels of protegrin-1 suggest a common subunit organization motif shared with toxic Alzheimer β-amyloid ion channels, Biophys. J. 95 (2008) 4631–4642.
[37] R. Capone, M. Mustata, H. Jang, F.T. Arce, R. Nussinov, R. Lal, Antimicrobial protegrin-1 forms ion channels: Molecular dynamic simulation, atomic force microscopy, and electrical conductance studies, Biophys. J., 98 2644–2652.
[38] H. Wang, J. de Joannis, Y. Jiang, J.C. Gaulding, B. Albrecht, F. Yin, K. Khanna, J.T. Kindt, Bilayer edge and curvature effects on partitioning of lipids by tail length: atomistic simulations, Biophys. J. 95 (2008) 2647–2657.
[39] R.L. Fahrner, T. Dieckmann, S.S. Harwig, R.I. Lehrer, D. Eisenberg, J. Feigon, Solution structure of protegrin-1, a broad-spectrum antimicrobial peptide from porcine leukocytes, Chem. Biol. 3 (1996) 543–550.
[40] A.S. Muresan, K.Y.C. Lee, Shape evolution of lipid bilayer patches adsorbed on mica: an atomic force microscopy study, J. Phys. Chem. B 105 (2001) 852–855.
[41] G. Schwarz, Thermodynamics and kinetics of incorporation into a membrane, Biochimie 71 (1989) 3–9.
[42] H.J.C. Berendsen, D. van der Spoel, R. van Drunen, Gromacs — a message-passing parallel molecular-dynamics implementation, Comput. Phys. Commun. 91 (1995) 43–56.
[43] E. Lindahl, B. Hess, D. van der Spoel, GROMACS 3.0: a package for molecular simulation and trajectory analysis, J. Mol. Model. 7 (2001) 306–317.
[44] D. van der Spoel, E. Lindahl, B. Hess, G. Groenhof, A.E. Mark, H.J.C. Berendsen, GROMACS: fast, flexible, and free, J. Comput. Chem. 26 (2005) 1701–1718.
[45] W. Humphrey, A. Dalke, K. Schulten, VMD: visual molecular dynamics, J. Mol. Graph. 14 (1996) 33–38.
[46] W.L. Jorgensen, J. Tirado-Rives, The OPLS potential functions for proteins — energy minimizations for crystals of cyclic-peptides and crambin, J. Am. Chem. Soc. 110 (1988) 1657–1666.
[47] O. Berger, O. Edholm, F. Jahnig, Molecular dynamics simulations of a fluid bilayer of dipalmitoylphosphatidylcholine at full hydration, constant pressure, and constant temperature, Biophys. J. 72 (1997) 2002–2013.
[48] D.P. Tieleman, J.L. MacCallum, W.L. Ash, C. Kandt, Z.T. Xu, L. Monticelli, Membrane protein simulations with a united-atom lipid and all-atom protein model: lipid–protein interactions, side chain transfer free energies and model proteins, J. Phys. Condens. Matter 18 (2006) S1221–S1234.
[49] W.L. Jorgensen, J. Chandrasekhar, J.D. Madura, R.W. Impey, M.L. Klein, Comparison of simple potential functions for simulating liquid water, J. Chem. Phys. 79 (1983) 926–935.
[50] U. Essmann, L. Perera, M.L. Berkowitz, T. Darden, H. Lee, L.G. Pedersen, A smooth particle mesh Ewald method, J. Chem. Phys. 103 (1995) 8577–8593.
[51] S. Miyamoto, P.A. Kollman, SETTLE — an analytical version of the shake and rattle algorithm for rigid water models, J. Comput. Chem. 13 (1992) 952–962.
[52] B. Hess, H. Bekker, H.J.C. Berendsen, J.G.E.M. Fraaije, LINCS: a linear constraint solver for molecular simulations, J. Comput. Chem. 18 (1997) 1463–1472.
[53] S.K. Kandasamy, R.G. Larson, Molecular dynamics simulations of model transmembrane peptides in lipid bilayers: a systematic investigation of hydrophobic mismatch, Biophys. J. 90 (2006) 2326–2343.
[54] Y. Jiang, H. Wang, J.T. Kindt, Atomistic simulations of "bicelles", Biophys. J. 98 (2010) 2895–2903.
[55] A. Saitoh, K. Takiguchi, Y. Tanaka, H. Hotani, Opening-up of liposomal membranes by alin, Proc. Natl. Acad. Sci. 95 (1998) 1026–1031.
[56] P.H. Puech, N. Borghi, E. Karatekin, F. Brochard-Wyart, Line thermodynamics: adsorption at a membrane edge, Phys. Rev. Lett. 90 (2003) 128304.
[57] P. Chen, The line adsorption equation: the one-dimensional counterpart of the Gibbs adsorption equation, Colloids Surf. A Physicochem. Eng. Asp. 161 (2000) 23–30.
[58] H. Leontiadou, A.E. Mark, S.J. Marrink, Antimicrobial peptides in action, J. Am. Chem. Soc. 128 (2006) 12156–12161.
[59] L. van Dam, G. Karlsson, K. Edwards, Direct observation and characterization of DMPC/DHPC aggregates under conditions relevant for biological solution NMR, Biochim. Biophys. Acta (BBA) - Biomembr. 1664 (2004) 241–256.
[60] K.L.H. Lam, The Mechanism of Membrane Disruption by Antimicrobal Microbial Peptide, in: Ph.D. Thesis, University of Chicago, 2009.
[61] K.Y.C. Lee, A. Gopal, A. von Nahmen, J.A. Zasadzinski, J. Majewski, G.S. Smith, P.B. Howe, K. Kjaer, Influence of palmitic acid and hexadecanol on the phase transition temperature and molecular packing of dipalmitoylphosphatidyl-choline monolayers at the air–water interface, J. Chem. Phys. 116 (2002) 774–783.
[62] J.J. Buffy, T. Hong, S. Yamaguchi, A.J. Waring, R.I. Lehrer, M. Hong, Solid-state NMR investigation of the depth of insertion of protegrin-1 in lipid bilayers using paramagnetic Mn^{2+}, Biophys. J. 85 (2003) 2363–2373.
[63] A.J. Waring, J.J. Buffy, R.I. Lehrer, M. Hong, Immobilization and aggregation of the antimicrobial peptide protegrin-1 in lipid bilayers investigated by solid-state NMR, Biochemistry 42 (2003) 13725–13734.
[64] J.J. Buffy, R. Mani, A.J. Waring, R.I. Lehrer, M. Hong, Solid-state NMR investigation of the selective disruption of lipid membranes by protegrin-1, Biochemistry 43 (2004) 13839–13848.
[65] S. Yamaguchi, T. Hong, A. Waring, R.I. Lehrer, M. Hong, Solid-state NMR investigations of peptide–lipid interaction and orientation of a beta-sheet antimicrobial peptide, protegrin, Biochemistry 41 (2002) 9852–9862.
[66] R. Mani, S.D. Cady, M. Tang, A.J. Waring, R.I. Lehrer, M. Hong, Membrane-dependent oligomeric structure and pore formation of a beta-hairpin antimicrobial peptide in lipid bilayers from solid-state NMR, Proc. Natl. Acad. Sci. 103 (2006) 16242–16247.
[67] R. Mani, A.J. Waring, R.I. Lehrer, M. Hong, Membrane-disruptive abilities of beta-hairpin antimicrobial peptides correlate with conformation and activity: a ^{31}P and ^{1}H NMR study, Biochim. Biophys. Acta (BBA) - Biomembr. 1716 (2005) 11–18.
[68] C. Roumestand, V. Louis, A. Aumelas, G. Grassy, B. Calas, A. Chavanieu, Oligomerization of protegrin-1 in the presence of DPC micelles. A proton high-resolution NMR study, FEBS Lett. 421 (1998) 263–267.
[69] J.J. Buffy, A.J. Waring, R.I. Lehrer, M. Hong, Immobilization and aggregation of the antimicrobial peptide protegrin-1 in lipid bilayers investigated by solid-state NMR, Biochemistry 42 (2003) 13725–13734.
[70] J.J. Buffy, A.J. Waring, M. Hong, Determination of peptide oligomerization in lipid bilayers using ^{19}F spin diffusion NMR, J. Am. Chem. Soc. 127 (2005) 4477–4483.
[71] M. Tang, A.J. Waring, M. Hong, Intermolecular packing and alignment of a β-hairpin antimicrobial peptide aggregate from 2D solid-state NMR, J. Am. Chem. Soc. 127 (2005) 13919–13927.
[72] R. Mani, M. Tang, X. Wu, J.J. Buffy, A.J. Waring, M.A. Sherman, M. Hong, Membrane-bound dimer structure of a β-hairpin antimicrobial peptide from rotational-echo double-resonance solid-state NMR, Biochemistry 45 (2006) 8341–8349.
[73] C.E. Miller, J. Majewski, E.B. Watkins, D.J. Mulder, T. Gog, T.L. Kuhl, Probing the local order of single phospholipid membranes using grazing incidence X-ray diffraction, Phys. Rev. Lett. 100 (2008) 058103.
[74] G. Wu, J. Majewski, C. Ege, K. Kjaer, M.J. Weygand, K.Y.C. Lee, Interaction between lipid monolayers and poloxamer 188: an X-ray reflectivity and diffraction study, Biophys. J. 89 (2005) 3159–3173.
[75] F. Jean-François, J. Elezgaray, P. Berson, P. Vacher, E.J. Dufourc, Pore formation induced by an antimicrobial peptide: electrostatic effects, Biophys. J. 95 (2008) 5748–5756.